

# Spin-Density-Wave Phase Transitions in Quasi-One-Dimensional Dimerized Quarter-Filled Organic Conductors

Jun-ichiro Kishine\* and Kenji Yonemitsu

*Department of Theoretical Studies, Institute for Molecular Science, Okazaki 444-8585, Japan*

(Received February 25, 1999)

We have studied spin density wave (SDW) phase transitions in dimerized quarter-filled Hubbard chains weakly coupled via interchain one-particle hopping,  $t_{b0}$ . It is shown that there exists a critical value of  $t_{b0}$ ,  $t_b^*$ , between the incoherent metal regime ( $t_{b0} < t_b^*$ ) and the Fermi liquid regime ( $t_{b0} > t_b^*$ ) in the metallic phase above the SDW transition temperature. By using the 2-loop perturbative renormalization-group approach together with the random-phase-approximation, we propose a SDW phase diagram covering both of the regimes. The SDW phase transition from the incoherent metal phase for  $t_{b0} < t_b^*$  is caused by growth of the intrachain electron-electron umklapp scattering toward low temperatures, which is regarded as preformation of the Mott gap. We discuss relevance of the present result to the SDW phase transitions in the quasi-one-dimensional dimerized quarter-filled organic conductors,  $(\text{TMTTF})_2\text{X}$  and  $(\text{TMTSF})_2\text{X}$ .

**KEYWORDS:** dimerization, umklapp scattering, interchain hopping, incoherent metal, Fermi liquid, spin density wave, perturbative renormalization-group

## §1. Introduction

Interplay of quantum fluctuations and dimensionality effects in quasi-one-dimensional (Q1D) organic conductors  $(\text{TMTTF})_2\text{X}$  and  $(\text{TMTSF})_2\text{X}$  ( $\text{X}=\text{Br}, \text{PF}_6, \dots$ ) has been extensively studied from both experimental and theoretical sides over the past two decades.<sup>1)</sup> Especially, different nature of the metallic phases above the spin-density-wave transition temperatures of  $(\text{TMTTF})_2\text{Br}$  and  $(\text{TMTSF})_2\text{PF}_6$  at ambient pressure has provoked a great deal of controversy. These compounds, in common, consist of quarter-filled chains with dimerized one-particle hopping integrals along the chain ( $a$ -axis),  $t_{a1}$  and  $t_{a2}$ , and an interchain one-particle hopping integral,  $t_b$ , along the intermediately conducting axis ( $b$ -axis). Hopping integrals along the third direction ( $c$ -axis) in both compounds are about one tenth of  $t_b$ .

Direct evidence of different nature of the metallic phases in the TMTTF and TMTSF compounds has been given by the optical reflectivity measurements which indicate the one-particle motion is

---

\* E-mail:kishine@ims.ac.jp

nearly confined into the chains in  $(\text{TMTTF})_2\text{Br}$ , while deconfined in  $(\text{TMTSF})_2\text{PF}_6$ .<sup>2,3)</sup> Temperature dependence of the  $a$ -axis resistivity in  $(\text{TMTTF})_2\text{Br}$  shows a shallow minimum around the so-called charge localization temperature and has been interpreted as preformation of a charge localization gap (Mott gap).<sup>4)</sup> On the other hand, it has been widely accepted that, as temperature decreases,  $(\text{TMTSF})_2\text{PF}_6$  undergoes a crossover to a Fermi liquid (FL) regime and the SDW phase transition in  $(\text{TMTSF})_2\text{PF}_6$  is driven by the Fermi surface nesting,<sup>5,6,7)</sup> below the crossover temperature. Although experimental assignment of the crossover temperature is still highly controversial,<sup>8,9,10)</sup> existence of the robust Fermi surface in the TMTSF compounds has also been supported through the success of the explanation of the field-induced SDW phenomena in the Fermiology scheme.<sup>11,12,13)</sup> Dimensionality effects on the SDW phase transition was also studied in  $(\text{TMTTF})_2\text{Br}$  under pressure  $P$ , indicating that  $T_N$  increases for  $P < P_{\text{opt}} = 5\text{kbar}$ , while decreases for  $P > P_{\text{opt}}$  and the crossover between the two regimes is roughly coincident with vanishing of the charge localization temperature.<sup>14,15)</sup> Similar pressure dependence was also observed in  $(\text{TMTTF})_2\text{PF}_6$ .<sup>8)</sup>

Q1D conductors behave as 1D systems at high temperatures,  $T \gg t_{b0}$ , where  $t_{b0}$  is a bare inter-chain one-particle hopping integral. Low-energy asymptotic behavior of 1D systems has been well understood by way of the renormalization-group (RG) approach based on the scaling hypothesis.<sup>16)</sup> In the absence of  $t_{b0}$ , due to the electron-electron umklapp scattering, the dimerized quarter-filled chain is scaled to a Mott insulator,<sup>17)</sup> which is characterized by the Mott gap and the antiferromagnetic power-law correlation. In the presence of small  $t_{b0}$ , as the temperature decreases, there occur the interchain one-particle propagation through the  $t_{b0}$  process and the propagation of the 1D antiferromagnetic (1DAF) power-law correlation through the interchain particle-hole exchange (ICEX) processes. The former process drives the crossover to the FL regime, while the latter process converts the 1DAF power-law correlation to the 2D (or 3D) long-range correlation. Since the latter process occurs *irrespective of the interchain quasiparticle coherence*, a phase transition from an “incoherent metal phase” occurs, if the latter dominates the former. The ICEX mechanism of phase transitions in Q1D systems was pointed out by Brasovskii and Yakobwenko,<sup>18)</sup> and confirmed by Suzumura.<sup>19)</sup>

So far, importance of the umklapp scattering and the resultant Mott gap in the TMTTF compounds has been extensively discussed,<sup>20,21,22,23,24,25,26,27)</sup> in terms of the weak-coupling RG approach. Bourbonnais<sup>23)</sup> argued that in the case of the TMTTF a coherent interchain one-particle hopping is prohibited due to formation of the Mott gap. Consequently the interchain AF interaction strength is given by  $J_{\perp} \sim v_F \tilde{t}_b^2 / \Delta_{\rho}^2$ , where  $\tilde{t}_b$  is a renormalized interchain one-particle hopping integral and  $\Delta_{\rho}$  is the preformed Mott gap which was introduced phenomenologically. Then the Stoner criteria gives the Néel temperature,  $T_N \sim \tilde{t}_b^2 / \Delta_{\rho}$ , which increases when  $\tilde{t}_b$  increases or  $\Delta_{\rho}$  decreases under pressure. Based on the bosonization approach, Suzumura *et al.*<sup>25,26,27)</sup> discussed a confinement-deconfinement transition in the half-filled two coupled chains in terms of a misfit parameter due to the interchain one-particle hopping integral and the Mott gap of the isolated half-filled chain at  $T = 0$ .

In the present paper, we extend the work shortly presented previously<sup>28)</sup> and discuss the SDW phase transitions from both the incoherent metal and the FL regimes in the dimerized quarter-

filled Hubbard chains weakly-coupled via the interchain one-particle hopping,  $t_{b0}$ . Based on the 2-loop RG approach, we show that there exists a critical value of  $t_{b0}$ ,  $t_b^*$ , between the incoherent metal regime ( $t_{b0} < t_b^*$ ) and the Fermi liquid regime ( $t_{b0} > t_b^*$ ) in the metallic phase above the SDW transition temperature. We assume that the scaling hypothesis in the 1D regime works well down to the SDW phase transition temperature for  $t_{b0} < t_b^*$  and determine the transition temperature,  $T_N^{\text{RG}}$ , based solely on the 2-loop renormalization-group flows, without introducing the preformed Mott gap phenomenologically. In the present framework, *growth of the umklapp scattering toward low temperatures plays an essential role on occurrence of the SDW phase transition from the incoherent metal phase*. As we shall discuss in §5, growth of the umklapp scattering strength is regarded as the preformation of the Mott gap and thus our results are consistent with the views based on the Mott gap.<sup>20, 21, 22, 23, 24, 25, 26, 27)</sup>

Outline of the present paper is as follows. In §2, we give a full account of the 2-loop RG treatment for the intra- and inter-chain processes and determine  $T_N^{\text{RG}}$  and  $t_b^*$ . In §3, the nesting-driven SDW phase transition in the FL regime is discussed based on the random-phase-approximation (RPA). In §4, we give a phase diagram covering both of the regimes,  $t_{b0} < t_b^*$  and  $t_{b0} > t_b^*$ . In §5, we discuss relevance of the present work to the views based on the Mott gap. We also comment on the problems which remain unsettled in the present scheme. Finally we conclude our work. In this work, we concentrate on the SDW phase transitions and do not discuss the spin-fluctuation-mediated superconducting phase transition which has been extensively discussed by several authors.<sup>6, 7, 29)</sup>

## §2. SDW Phase Transition from the Incoherent Metal Regime

### 2.1 Model and effective Hamiltonian

We consider an array of a large number of dimerized quarter-filled Hubbard chains on the a-b plane (Fig. 1). The nearest neighbor chains are weakly coupled via the interchain one-particle hopping  $t_{b0}$ . The dimerization along the  $a$ -axis and the intrachain on-site Coulomb repulsion,  $U$ , are taken into account. As shown in Fig. 2, due to the dimerization the one-particle dispersion is split into the upper and lower bands given by

$$\pm\sqrt{t_{a1}^2 + t_{a2}^2 + 2t_{a1}t_{a2}\cos k_a - 2t_{b0}\cos k_b}, \quad (1)$$

where electron wave numbers along the a- and b-axes are denoted by  $k_a$  and  $k_b$ , respectively. In the temperature scale considered here, which is much smaller than the Fermi energy or intrachain one-particle hopping integrals, electron dynamics is confined into the effectively half-filled lower band. In the absence of  $t_{b0}$  and  $U$ , the dispersion relation, (1), gives the density of states per spin  $\mathcal{N}(\varepsilon) = -\frac{1}{2\pi t_{a1}t_{a2}}\varepsilon/\sqrt{1 - \{\varepsilon^2 - t_{a1}^2 - t_{a2}^2\}/2t_{a1}t_{a2}})^2$ , which relates the chemical potential,  $\mu$ , to the carrier density,  $n$  ( $n = 1$  corresponds to the half-filled lower band), as  $n = 1 - \frac{2}{\pi}\sin^{-1}[(t_{a1}^2 + t_{a2}^2 - \mu^2)/2t_{a1}t_{a2}]$ . Thus,  $n = 1$  corresponds to the Fermi wave number,  $k_F = \pi/2$ , and the Fermi velocity,  $v_F = t_{a1}t_{a2}/\sqrt{t_{a1}^2 + t_{a2}^2}$ . Taking account of modification of the Fermi wave number due to the weak dispersion in the b-axis direction, as was done in Refs.[6] and [11], we obtain the one-particle dispersion linearized in the  $k_a$ -direction at the Fermi points  $k_F$  as

$$\xi(\mathbf{k}) = v_F(|k_a| - k_F) - 2t_{b0}\cos k_b + 2t'_{b0}\cos 2k_b + \mathcal{O}(t_{b0}^3/t_{a1}^2), \quad (2)$$

where

$$t'_{b0} = \frac{t_{b0}^2}{W} \sqrt{\frac{2}{1 + \delta^2}}, \quad (3)$$

with  $W = 2(t_{a1} + t_{a2})$  and  $\delta = (t_{a1} - t_{a2})/(t_{a1} + t_{a2})$  being the total bandwidth and the dimerization ratio in the absence of  $t_{b0}$  and  $U$ . The third term of (2), breaks the perfect nesting of the Fermi surface.

In the absence of  $t_{b0}$ , the one-particle thermal coherence length along the  $a$ -axis is given by  $\xi_a = v_F/T$  with  $T$  being the temperature,<sup>30)</sup> and it becomes much larger than the intrachain lattice spacing at temperatures,  $T \ll v_F$ . This situation enables us to take the continuum limit along the  $a$ -direction and to apply the renormalization-group analysis to the intrachain system based on the *scaling hypothesis* in the 1D regime. On the other hand, since the temperature scale considered here can become comparable with the small perturbation,  $t_{b0}$ , the one-particle thermal coherence length along the  $b$ -axis becomes comparable with the distance between the adjacent chains. Thus *we must keep lattice discreteness along the  $b$ -axis*.

Based on the bandwidth regularization scheme, as shown in Fig. 2, we restrict the electron wave numbers *along the  $a$ -axis* to the regions

$$\mathcal{C}_l = \{k_a \mid -\omega_l/2 \leq \xi_\nu(k_a) \leq \omega_l/2\}, \quad (4)$$

where  $\xi_R(k_a) = v_F(k_a - k_F)$  ( $k_a > 0$ ) and  $\xi_L(k_a) = v_F(-k_a - k_F)$  ( $k_a < 0$ ) are the linearized dispersions for the right- and left-moving electrons. The cutoff of the linearized band is parameterized as  $\omega_l = E_0 e^{-l}$  with the scaling parameter,  $l$ . The cutoff energy  $\omega_l$  corresponds to a characteristic energy at which we observe the system. From now on we regard  $\omega_l$  as the temperature scale  $\omega_l \sim T$ . As  $l$  goes from zero to infinity, we move from high-temperature scales, where the system is regarded as the 1D chains, to low-temperature scales where the interchain couplings play important roles.

We start with the effective Hamiltonian which depends on the energy scale,  $l$ , as

$$\mathcal{H}_l = \mathcal{H}_{a;l}^{(1)} + \mathcal{H}_{a;l}^{(2)} + \mathcal{H}_{b;l}^{(1)} + \mathcal{H}_{b;l}^{(2)}, \quad (5)$$

which are described below. The intrachain one-particle term is written as

$$\mathcal{H}_{a;l}^{(1)} = \sum_{i=1}^{N_b} \sum_{k_a \in \mathcal{C}_l} \sum_{\sigma} \left[ \xi_R(k_a) R_{i,\sigma}^*(k_a) R_{i,\sigma}(k_a) + \xi_L(k_a) L_{i,\sigma}^*(k_a) L_{i,\sigma}(k_a) \right], \quad (6)$$

where  $R_{i,\sigma}$  ( $R_{i,\sigma}^*$ ) and  $L_{i,\sigma}$  ( $L_{i,\sigma}^*$ ) are fermion annihilation (creation) operators representing the right- and left-moving electrons, respectively, on the  $i$ -th chain in the vicinity of the Fermi points in the lower band, and  $N_b$  is the number of the chains. As will be discussed in §2.2 and the Appendix, the scale-invariance under the renormalization transformation in the 1D regime is imposed on  $\mathcal{H}_{a;l}^{(1)}$ .

The interchain one-particle process [Fig. 3 (a)] is renormalized through the intrachain self-energy effects,<sup>20)</sup> and consequently become dependent on the energy-scale. By introducing the Fourier transform,  $R_{i,\sigma}(k_a) = \frac{1}{\sqrt{N_b}} \sum_{k_b} e^{ik_b i} R(\mathbf{k})$  with  $\mathbf{k} = (k_a, k_b)$ , and  $L_{i,\sigma}(k_a)$  likewise, the interchain one-particle term is written as

$$\mathcal{H}_{b;l}^{(1)} = -2t \sum_{k_a \in \mathcal{C}_l} \sum_{-\pi \leq k_b \leq \pi} \sum_{\sigma} (t_{b;l} \cos k_b - t'_{b;l} \cos 2k_b) [R_{\sigma}^*(\mathbf{k}) R_{\sigma}(\mathbf{k}) + L_{\sigma}^*(\mathbf{k}) L_{\sigma}(\mathbf{k})]. \quad (7)$$

Unrenormalized values of  $t_{b;l}$  and  $t'_{b;l}$  are denoted by  $t_{b0}$  and  $t'_{b0}$ , respectively.

The intrachain two-particle scattering processes contain the normal [Fig. 3(b),(c)] and umklapp [Fig. 3(d)] processes with the dimensionless scattering strengths,  $g_l^{\sigma_1\sigma_2\sigma_3\sigma_4}$  and  $g_{3;l}$ , respectively.<sup>16)</sup> The corresponding term is written as

$$\begin{aligned} \mathcal{H}_{a;l}^{(2)} &= \frac{\pi v_F}{N_a} \sum_{i=1}^{N_b} \sum_{k_{ai} \in C_l} \sum_{\sigma_i} g_l^{\sigma_1\sigma_2\sigma_3\sigma_4} R_{i,\sigma_1}^*(k_{a1}) L_{i,\sigma_2}^*(k_{a2}) L_{i,\sigma_3}(k_{a3}) R_{i,\sigma_4}(k_{a4}) \\ &+ \frac{\pi v_F}{2N_a} g_{3;l} \sum_i \sum_{k_{ai} \in C_l} \sum_{\sigma, \sigma'} \left[ R_{i,\sigma}^*(k_{a1}) R_{i,\sigma'}^*(k_{a2}) L_{i,\sigma'}(k_{a3}) L_{i,\sigma}(k_{a4}) + \text{c.c.} \right], \end{aligned} \quad (8)$$

where  $N_a$  denotes the number of sites in the chain. The summation over momentum is taken under the constraint:  $k_{a1} + k_{a2} - k_{a3} - k_{a4} = G$  with  $G = 0$  and  $G = \pm 4k_F = \pm 2\pi$  for the normal and umklapp processes, respectively. The normal scattering is decomposed into backward [Fig. 3(b)] and forward [Fig. 3(c)] scattering as

$$g_l^{\sigma_1\sigma_2\sigma_3\sigma_4} = \delta_{\sigma_1\sigma_4} \delta_{\sigma_2\sigma_3} g_{2;l} - \delta_{\sigma_1\sigma_3} \delta_{\sigma_2\sigma_4} g_{1;l}, \quad (9)$$

where the forward and backward scattering strengths are denoted by  $g_{2;l}$  and  $g_{1;l}$ , respectively. Unrenormalized scattering strengths are related to the on-site Coulomb repulsion,  $U$ , as<sup>17)</sup>

$$\pi v_F g_{1;0} = \frac{U}{2}, \quad \pi v_F g_{2;0} = \frac{U}{2}, \quad \pi v_F g_{3;0} = \frac{U}{2} \frac{2\delta}{1 + \delta^2}. \quad (10)$$

The umklapp scattering strength depends on the dimerization ratio,<sup>17)</sup> in contrast with the half-filled case.

By multiple use of the interchain one-particle hopping and the intrachain two-particle interaction, the ICEX processes are dynamically generated during the renormalization.<sup>18,20)</sup> As described below, we consider only the case where the most dominant 1D power-law correlation is an antiferromagnetic one. In this case, as in the weakly-coupled half-filled chain system,<sup>31)</sup> the most dominant ICEX process is in the AF channel. The corresponding term is written as

$$\begin{aligned} \mathcal{H}_{b;l}^{(2)} &= \frac{\pi v_F}{N_a} \sum_{i \neq j} \sum_{q_a} J_{i-j;l} \mathbf{S}_i(q_a) \cdot \mathbf{S}_j^*(q_a) \\ &+ \frac{\pi v_F}{N_a} \sum_{i \neq j} \sum_{q_a} K_{i-j;l} [\mathbf{S}_i(2k_F + q_a) \cdot \mathbf{S}_j(2k_F - q_a) + \text{c.c.}] \end{aligned} \quad (11)$$

where  $J_{i-j;l}$  and  $K_{i-j;l}$  represent the strengths of interaction between the  $i$ -th and  $j$ -th chains through the normal and umklapp scattering, respectively [see Fig. 3(e) and 3(f)]. It should be noted that, in the presence of the intrachain umklapp process, we have to include the  $K_{i-j;l}$ -process which was not taken into account in Ref.[21]. The  $2k_F$  spin-density on the  $i$ -th chain is given by

$$\mathbf{S}_{i;l}(q_a) = \sum_{\substack{k_a \in C_l \\ k_a + q_a \in C_l}} R_{i,\alpha}^*(k_a + q_a) \frac{\sigma_{\alpha\beta}}{2} L_{i,\beta}(k_a). \quad (12)$$

The interaction strengths are initially zero,

$$J_{i-j;0} = K_{i-j;0} = 0, \quad (13)$$

but dynamically generated during the renormalization process. By taking the Fourier transforms,  $J_{q_b;l} = \frac{1}{N_b} \sum_{i \neq j} e^{iq_b(i-j)} J_{i-j;l}$ ,  $K_{q_b;l} = \frac{1}{N_b} \sum_{i \neq j} e^{iq_b(i-j)} K_{i-j;l}$  and  $\mathbf{S}_l(q_a, q_b) = \frac{1}{N_b} \sum_{q_b} e^{iq_b i} \mathbf{S}_{i;l}(q_a)$ , the term, (11), is rewritten as

$$\begin{aligned} \mathcal{H}_{b;l}^{(2)} &= \frac{\pi v_F}{N_a N_b} \sum_{q_a, q_b} J_{q_b;l} \mathbf{S}_l^*(q_a, q_b) \cdot \mathbf{S}_l(q_a, q_b) \\ &+ \frac{\pi v_F}{N_a N_b} \sum_{q_a, q_b} K_{q_b;l} [\mathbf{S}_l(2k_F + q_a, q_b) \cdot \mathbf{S}_l(2k_F - q_a, -q_b) + \text{c.c.}] \end{aligned} \quad (14)$$

## 2.2 Renormalization-group equations

The PRG approach<sup>20)</sup> is based on the assumption that  $g_{i;l}$  and  $t_{b;l}$  are considerably smaller than  $E_0$  and sets up low-order scaling equations whose solutions indicate whether these small perturbations grow toward the low-energy scales or not. During this step, we take account of the intrachain scattering and self-energy processes at the 2-loop level. Outline of the derivation of the RG equations is left to the Appendix.

Renormalization of the interchain one-particle hopping comes solely from the intrachain self-energy processes and the corresponding RG equations are given by<sup>20, 21, 22)</sup>

$$\frac{d}{dl} \ln t_{b;l} = 1 - \theta_l, \quad (15)$$

$$\frac{d}{dl} \ln t'_{b;l} = 1 - \theta_l, \quad (16)$$

where a non-universal exponent  $\theta_l$  comes from the intrachain self-energy processes as shown in Fig. 4 and is given by<sup>32, 21)</sup>

$$\theta_l = \frac{1}{4} [g_{1;l}^2 + g_{2;l}^2 - g_{1;l}g_{2;l} + g_{3;l}^2/2]. \quad (17)$$

During the renormalization process, no new interchain one-particle hopping is generated. We see from eqs. (15) and (16) that the ratio  $t'_{b;l}/t_{b;l}$  is scale-invariant:

$$t'_{b;l}/t_{b;l} = t'_{b0}/t_{b0} = \frac{t_{b0}}{W} \sqrt{\frac{2}{1 + \delta^2}}. \quad (18)$$

The 2-loop RG equations for the intrachain normal and umklapp scattering strengths are given by<sup>32, 16)</sup>

$$\frac{d}{dl} g_{1;l} = -g_{1;l}^2 - \frac{1}{2} g_{1;l}^3, \quad (19)$$

$$\frac{d}{dl} G_l = -g_{3;l}^2 \left(1 + \frac{1}{2} G_l\right), \quad (20)$$

$$\frac{d}{dl} g_{3;l} = -g_{3;l} G_l \left(1 + \frac{1}{4} G_l\right) - \frac{1}{4} g_{3;l}^3, \quad (21)$$

where  $G_l = g_{1;l} - 2g_{2;l}$ . The intrachain charge degrees of freedom are governed by the combination  $(G_l, g_{3;l})$  with flow lines  $(G_l - \text{const.})^2 - g_{3;l}^2 = \text{const.}$ . When the unrenormalized values,  $G_0$  and  $g_{3;0}$  satisfy the condition,

$$G_0 < |g_{3;0}|, \quad (22)$$

the umklapp process becomes relevant and the 2-loop RG eqs. (19)  $\sim$  (21) give the non-trivial fixed point,  $g_{1;\infty} = 0$  and  $|g_{3;\infty}| = -G_\infty = 2$ .<sup>16)</sup> In the absence of the interchain coupling, the low-energy asymptotics is a Mott insulator with the dominant AF power-law correlation.<sup>16)</sup> As far as the condition (22) is satisfied, all the results described below are qualitatively unchanged. Thus, from now on except in Figs. 8 and 13 shown below, we fix  $U$  at  $U = 1.45\pi v_F$  which corresponds to  $g_{1;0} = g_{2;0} = 0.725$  and  $g_{3;0} = 0.725 \times 2\delta/(1 + \delta^2)$ .

We note that the non-trivial fixed point,  $g_{1;\infty} = 0$  and  $|g_{3;\infty}| = -G_\infty = 2$ , gives

$$d \ln t_{b;l} / dl \xrightarrow{l \rightarrow \infty} 1/4. \quad (23)$$

Thus, for large  $l$ ,  $t_{b;l}$  grows as  $t_{b;l} = t_{b0} e^{l/4}$ . Consequently,  $t_b$  is a *relevant* perturbation in the RG sense and always attains an order of the initial bandwidth,  $E_0$ , at some crossover value of the scaling parameter qualitatively defined by  $t_{b;l_{\text{cross}}} = E_0$ . Here we stress that *the relevance or irrelevance of  $t_{b;l}$  in the asymptotic limit of the RG flow makes no qualitative difference on the crossover to the FL regime at a finite energy scale*. Actually, the 1-loop RG analysis gives the strong coupling fixed point  $|g_{3;\infty}| = -G_\infty = \infty$ <sup>16)</sup> and accordingly  $t_{b;l}$  becomes irrelevant [see eq. (15)]. In this case the flow of  $\theta_l$  deviates from that obtained by the 2-loop analysis given here only at energy scales much lower than  $T_{\text{cross}}$  defined below by eq. (24). This is the very reason why it is important to *keep track of the whole RG flow of  $t_{b;l}$* .

The temperature scale,

$$T_{\text{cross}} = E_0 e^{-l_{\text{cross}}}, \quad (24)$$

gives a qualitative measure around which the interchain one-particle motion begins to develop.<sup>33)</sup> In Fig. 5, we show the RG flows of  $t_{b;l}$  for various dimerization ratios,  $\delta = 0.05, 0.2, 0.4, 0.6, 0.8$ . We see that finite dimerization strongly suppresses the growth of  $t_{b;l}$ , since the increasing  $\delta$  causes the stronger umklapp scattering which suppresses more and more severely the interchain one-particle propagation.

In Figs. 6(a) and 6(b), we show contribution to the RG equations for the ICEX processes in the AF channel for the normal and umklapp scattering processes, respectively. The respective equations are given by

$$\begin{aligned} \frac{d}{dl} J_{q_b;l} &= \frac{1}{2} \left[ g_{2;l}^2 + 4g_{3;l}^2 \right] f_l(q_b) \\ &+ \frac{1}{2} [(g_{2;l} - 4\theta_l) J_{q_b;l} + 4g_{3;l} K_{q_b;l}] - \frac{1}{4} \left[ J_{q_b;l}^2 + 4K_{q_b;l}^2 \right], \end{aligned} \quad (25)$$

$$\frac{d}{dl} K_{q_b;l} = 2g_{2;l} g_{3;l} f_l(q_b) + 2[(g_{2;l} - \theta_l) K_{q_b;l} + g_{3;l} J_{q_b;l}] - J_{q_b;l} K_{q_b;l}, \quad (26)$$

where

$$\begin{aligned} f_l(q_b) &= \tilde{t}_{b;l}^2 \cos q_b + \tilde{t}_{b;l}^{\prime 2} \cos 2q_b \\ &= \tilde{t}_{b;l}^2 \left[ \cos q_b + \left( \frac{t'_{b0}}{t_{b0}} \right)^2 \cos 2q_b \right] \end{aligned} \quad (27)$$

with  $\tilde{t}_{b;l} = t_{b;l}/E_0$  and  $\tilde{t}_{b;l}' = t'_{b;l}/E_0$ . Figs. 6(a-1) and 6(b-1) represent the dynamical generation of these processes and give the first terms of (25) and (26). Figs. 6(a-2) and 6(b-2) represent the

coupling of the intrachain AF process to the interchain process and give the second terms of (25) and (26). Figs. 6(a-3) and 6(b-3) represent the coupling of the interchain processes themselves and give the third terms of (25) and (26).

Although the unrenormalized values of  $J_{q_b;0}$  and  $K_{q_b;0}$  are zero, the first terms of eqs.(25) and (26) generate finite magnitudes of  $J_{q_b;l}$  and  $K_{q_b;l}$ , then the second terms induce their exponential growth, and finally the third terms cause their divergence at the critical scaling parameter  $l_c$  which depends on the momentum  $q_b$  in the  $b$ -axis direction,  $J_{q_b;l_c(q_b)} = K_{q_b;l_c(q_b)} = -\infty$ . The divergence corresponds to the phase transition to the long-range ordered phase at temperature,  $T_N^{\text{RG}}(q_b) = E_0 e^{-l_c(q_b)}$ . At the most favorable SDW vector,  $f_l(q_b)$  becomes negative and has a maximum absolute value. This vector is always given by  $q_b = \pi$ , when the small  $t_{b0}$  satisfies  $t'_{b0}/t_{b0} = \frac{t_{b0}}{W} \sqrt{\frac{2}{1+\delta^2}} < 1/2$ . Thus, within the present scheme, the ICEX mechanism causes the commensurate SDW state characterized by the SDW vector,

$$\mathbf{Q}_{\text{RG}} = (2k_F, \pi), \quad (28)$$

with  $k_F = \pi/2$ . From now on, we fix  $q_b = \pi$  in  $J_{q_b;l}$  and  $K_{q_b;l}$  and introduce the SDW transition temperature,

$$T_N^{\text{RG}} = E_0 e^{-l_N}, \quad (29)$$

with  $l_N = l_c(\pi)$ . In our formulation, contribution from the interchain processes to the intrachain processes are not taken into account. As a result, the present treatment of the phase transition is analogous to the interchain mean-field theory of quasi-one-dimensional systems.<sup>34)</sup>

As is seen from the diagrams in Figs. 6(a) and (b), the intrachain umklapp processes couple strongly to the ICEX processes. Consequently, growth of the umklapp scattering toward low temperature strongly enhances the ICEX processes. On the other hand, as we previously noted, the umklapp scattering suppresses the interchain one-particle process. As a consequence of these combined effects, there appears a region where the SDW phase transition from the incoherent metal phase driven by the ICEX process dominates the interchain one-particle crossover to the FL regime. It is noted that, in the absence of the umklapp process, the one-particle crossover always dominates the ICEX-driven phase transition, provided  $U$  is not extremely large.<sup>33)</sup>

### 2.3 AF phase transition temperature and the critical value of $t_{b0}$

By solving the coupled RG equations (15), (19) ~ (21), (25) and (26) and keeping track of the RG flows of the interchain one- and two-particle processes at finite energy scales, we compare the growth of the interchain one-particle propagation through the  $t_{b0}$  process with that of the interchain propagation of the dominant 1DAF correlation through the ICEX process. When the RG equations give  $T_N > T_{\text{cross}}$ , the SDW phase transition driven by the ICEX mechanism occurs. Otherwise, evolution of 2D quasiparticle coherence leads the system to the 2D Fermi liquid (FL) regime.

In Figs. 7(a), 7(b), and 7(c) we show the RG flows of  $g_{3;l}$ ,  $t_{b;l}/E_0$ ,  $J_{q_b;l}$  and  $K_{q_b;l}$  with  $q_b = \pi$  for  $\delta = 0.2$  and  $t_{b0}/E_0 = 0.02, 0.108, 0.3$ , where the vertical lines show the locations of  $l_{\text{cross}}$  and  $l_N$ . RG flows of the umklapp scattering strength,  $g_{3;l}$ , depend only on the intrachain Hubbard repulsion,  $U$ , and grow toward the strong coupling fixed point,  $g_{3;\infty} = 2$ . We here assume that

the scaling procedure works well down to  $T_N^{\text{RG}}$ , although  $g_{3;l}$  exceeds unity at energy scales higher than  $T_N^{\text{RG}}$ . We see that  $l_{\text{cross}} > l_N$  (i.e.  $T_{\text{cross}} < T_N^{\text{RG}}$ ) for  $t_{b0} = 0.02E_0$ , while  $l_{\text{cross}} < l_N$  (i.e.  $T_{\text{cross}} > T_N^{\text{RG}}$ ) for  $t_{b0} = 0.3E_0$ . As is seen from Fig. 7(b),  $t_{b0} = t_b^* = 0.108E_0$  gives the critical value where  $l_{\text{cross}} = l_N$  (i.e.  $T_{\text{cross}} = T_N^{\text{RG}}$ ). In Fig. 8, dependence of  $t_b^*$  on the dimerization ratio  $\delta$  is shown for  $U/\pi v_F = 1.0, 1.45, 1.6$ . We see that a finite  $\delta$  causes a finite  $t_b^*$ . This situation arises, since  $\delta$  strengthens the intrachain umklapp scattering [see eq.(10)], and consequently more severely suppresses the interchain one-particle propagation. As  $U$  increases, overall magnitude of  $t_b^*$  increases, since the increasing  $U$  strengthens both the umklapp and mormal scattering and consequently enhances the ICEX mechanism.

### §3. Nesting-driven SDW phase Transition in the Fermi Liquid Regime

As discussed in the previous section, for  $t_b^* < t_{b0}$ , the system undergoes a crossover to the FL regime below  $T_{\text{cross}}$ . Inside the FL regime, the SDW phase transition is driven by the Fermi surface nesting. Except the region with  $t_{b0}$  very near the critical value,  $t_b^*$ , the nesting-driven SDW phase transition can be treated by the random-phase-approximation (RPA) where only unrenormalized particle-hole fluctuations are taken into account.<sup>5,6,7)</sup> Quite recently, Kino and Kontani treated the effects of the particle-hole fluctuations on the one-particle propagator in a consistent manner.<sup>35)</sup> Near the critical value, interference between the particle-particle and particle-hole polarization is expected to be so strong that the RPA treatment for the phase transition would be insufficient. In this work, to give a qualitative view on the different nature of the SDW transitions from the incoherent metal regime and from the FL regime, we simply treat the phase transition in the FL regime using the RPA.

In Fig. 9, we show a series of diagrams representing the particle-hole fluctuations which contribute to the transverse susceptibility. The longitudinal counterpart is given similarly. We here stress that, in Fig. 9, the unrenormalized one-particle propagator has a two-dimensional character as

$$\mathcal{G}_\nu^{\text{2D}}(\mathbf{k}, \varepsilon) = [i\varepsilon - v_F(|\mathbf{k}| - k_F) + 2t_b \cos k_b - 2t'_b \cos 2k_b]^{-1}, \quad (30)$$

where  $\nu = R$  or  $L$  and  $\varepsilon$  is a fermion thermal frequency. The SDW phase transition temperature,  $T_N^{\text{RPA}}$ , is determined through the condition for the dimensionless static particle-hole polarization function at an optimal nesting vector,  $\chi(T; t_{b0})$ ,

$$\begin{aligned} \chi(T_N^{\text{RPA}}; t_{b0}) &= [g_{2;0} + g_{3;0}]^{-1} \\ &= \pi v_F \left[ \frac{U}{2} \left( 1 + \frac{2\delta^2}{1 + \delta^2} \right) \right]^{-1}. \end{aligned} \quad (31)$$

The polarization function in the noninteracting case,  $\chi(T; t_{b0})$ , is given by

$$\begin{aligned} \chi(T; t_{b0}) &= -\pi v_F T \sum_{\substack{|\xi_R(k_a)| \leq E_0/2 \\ |k_b| \leq \pi}} \sum_{\varepsilon} \mathcal{G}_R^{\text{2D}}(\mathbf{k}, \varepsilon) \mathcal{G}_L^{\text{2D}}(\mathbf{k} - \mathbf{Q}, \varepsilon) \\ &= \frac{1}{4\pi} \int_{-E_0/2}^{E_0/2} d\xi_R \int_0^\pi dk_y \frac{\tanh[\xi(\mathbf{k})/2T] - \tanh[\xi(\mathbf{k} - \mathbf{Q})/2T]}{\xi(\mathbf{k}) - \xi(\mathbf{k} - \mathbf{Q})}, \end{aligned} \quad (32)$$

where we adopt the intrachain linearized bandwidth cutoff,  $E_0$ , to keep consistency with the treatment in the previous section.

In Fig.10, we show dependence of  $T_N^{\text{RPA}}$  on  $t_{b0}$  for  $\delta = 0.05, 0.2, 0.4$  in the case of the commensurate SDW vector,

$$\mathbf{Q} = (\pi, \pi). \quad (33)$$

We here put  $W = 8E_0$ .  $T_N^{\text{RPA}}$  is sharply suppressed at the critical values,  $t_{b0:\text{cr}}/E_0 \sim 0.30, 0.347, 0.39$ , for dimerization ratios,  $\delta = 0.05, 0.2, 0.4$ , respectively. Increasing  $t_{b0}$  weakens the degree of nesting through the third term of (2) and consequently reduces the transition temperature. As  $\delta$  decreases, overall magnitude of  $T_N^{\text{RPA}}$  decreases, since the decreasing  $\delta$  weakens the umklapp scattering strength and consequently reduces the effective two-particle interaction strength [see eq. (31)]. As pointed out by Hasegawa and Fukuyama,<sup>6)</sup> there exists a very narrow region of  $t_{b0}$  in the vicinity of  $t_{b0:\text{cr}}$  where an incommensurate SDW is favored, but we do not go into the minor details on this issue here.

#### §4. Phase Diagrams

By combining the results on  $T_N^{\text{RG}}$ ,  $T_{\text{cross}}$  and  $T_N^{\text{RPA}}$  in §3 and §4, we obtain a phase diagram covering both the incoherent metal regime and the FL regime. In Fig. 11, we show a phase diagram for  $\delta = 0.2$ ,  $U = 1.45\pi v_F$ . In this case,  $T_N^{\text{RG}}$  and  $T_N^{\text{RPA}}$  meet together around the critical value,  $t_{b0} = t_b^*$ . This choice of parameters is consistent with that of the TMTTF compound.<sup>36)</sup> As shown in Fig. 8,  $t_b^*$  is sensitive to both  $U$  and  $\delta$ . Thus, by tuning  $U$  and  $\delta$  appropriately, a phase diagram qualitatively similar to Fig. 11 is always obtained, as far as the low-energy asymptotics of the system without  $t_{b0}$  is a Mott insulator. The  $t_{b0}$ -dependence of the SDW phase transition temperature in the two regimes is interpreted as follows. For  $t_{b0} < t_b^*$ , the increasing  $t_{b0}$  enhances the interchain propagation of the dominant 1DAF correlation through the ICEX process toward low temperatures and consequently increases the SDW transition temperature. This situation is consistent with Bourbonnais' argument based on the preformed Mott gap,  $\Delta_\rho$ ,<sup>23)</sup> that the Stoner criteria gives the Néel temperature,  $T_N \sim \tilde{t}_b^2/\Delta_\rho$ , which increases when the renormalized interchain one-particle hopping integral,  $\tilde{t}_b$ , increases under pressure. On the other hand, once the system undergoes the crossover to the FL regime for  $t_{b0} > t_b^*$ , the increasing  $t_{b0}$  weakens the degree of nesting of the Fermi surface and consequently decreases the SDW transition temperature.

When we adopt dimerization ratios smaller or larger than  $\delta = 0.2$  with the same interaction strength as in Fig. 11, both  $T_N$  and  $T_N^{\text{RPA}}$  change accordingly and no longer meet together around the critical value,  $t_{b0} = t_b^*$ . As shown in Fig. 12,  $T_N^{\text{RPA}}$  excessively dominates  $T_N$  for  $\delta = 0.05$  [Fig. 12(a)], while the opposite situation occurs for  $\delta = 0.6$  [Fig. 12(b)]. In the case of  $\delta = 0.05$ , the intrachain umklapp scattering is much weaker than that in the case of  $\delta = 0.2$  and consequently the ICEX mechanism becomes ineffective over the wide range of  $t_{b0}$ . On the other hand, in the case of  $\delta = 0.6$ , the strong intrachain umklapp scattering enhances the ICEX mechanism. These misfits should be seen as an artifact originating from the following two facts. First, for  $t_{b0} < t_b^*$ , feedback effects of the interchain processes on the intrachain processes in the 1D regime have not taken into account within the present scheme. Secondly, for  $t_{b0} > t_b^*$ , we have treated the SDW phase transition in the simple RPA and have not taken account of the effects of strong quantum fluctuations in the vicinity of  $t_b^*$ . Concerning these points, we did not apply the renormalization-group (RG) procedure to the

$g_{2;l}$  and  $g_{3;l}$  processes in (31). However, in the vicinity of  $t_b^*$ , the RG treatment of  $g_{2;l}$  and  $g_{3;l}$  might still work.<sup>23)</sup> If these quantum-fluctuation effects are fully taken into account over the whole range of  $t_{b0}$ , the resultant SDW phase transition temperature is expected to exhibit a continuous change similar to Fig. 11. In any case, Fig. 12 suggests that the ICEX mechanism is more sensitive to the dimerization ratio,  $\delta$ , than the nesting mechanism.

Although our model considered here misses some details of real structure of the TMTTF and TMTSF compounds such as misfit between the adjacent chains, which is discussed in §5.2, our results are qualitatively consistent with the experimental suggestions that the metallic phases just above  $T_N$  in the TMTTF and TMTSF compounds at ambient pressure belong to the different regimes where the 2D (or 3D) quasiparticle coherence is present in  $(\text{TMTSF})_2\text{PF}_6$ , but absent in  $(\text{TMTTF})_2\text{Br}$ . As shown in Fig. 8, the critical value,  $t_b^*$ , is sensitive to the dimerization ratio,  $\delta$ , since  $\delta$  controls the intrachain umklapp scattering strength. This result suggests that, in the TMTTF compounds with larger dimerization ratio, the ICEX-driven SDW transition becomes effective up to a considerable magnitude of  $t_{b0}$ , while in the case of TMTSF with smaller dimerization ratio, the ICEX mechanism becomes ineffective even for rather small  $t_{b0}$ . This situation suggests that very small  $t_{b0}$  is sufficient for  $(\text{TMTSF})_2\text{PF}_6$  to evolve the interchain coherent one-particle motion and is consistent with the experimental suggestion and phenomenological discussion by Emery et al.<sup>4)</sup>

Roughly speaking, the increasing  $t_{b0}$  corresponds to increasing applied pressure. Thus our SDW phase diagram, Fig. 11, is consistent with the experimental observation in  $(\text{TMTTF})_2\text{Br}$  under pressure,  $P$ , where the transition temperature increases at  $P < P_{\text{opt}} = 5\text{kbar}$ , while decreases at  $P > P_{\text{opt}}$ .<sup>14)</sup>

## §5. Discussion

In this section, we discuss relevance of the present work to other ones and comment on the problems which remain unsettled in the present scheme.

### 5.1 Zero-temperature Mott gap

In the present paper, we have assumed the scaling hypothesis works well down to  $T_N^{\text{RG}}$  for  $t_{b0} < t_b^*$  and determined  $T_N^{\text{RG}}$  based solely on the 2-loop renormalization-group flows without introducing the preformed Mott gap. As stressed repeatedly, in our formulation, growth of the umklapp scattering toward low temperatures plays an essential role on occurrence of the SDW phase transition for  $t_{b0} < t_b^*$ . The growth of the umklapp scattering strength is regarded as preformation of the Mott gap. Thus our results are consistent with the views based on the Mott gap.<sup>20, 21, 22, 23, 24, 25, 26, 27)</sup>

To see this situation more closely, we here discuss the zero-temperature Mott gap of the isolated dimerized quarter-filled Hubbard chain in the weak-coupling regime:<sup>17, 37)</sup>

$$\Delta_{\rho 0}(U, \delta) = \frac{4v_F}{\pi} (1 - A^2)^{1/4} \exp \left[ -\frac{1}{4} \frac{\tanh^{-1} A}{A} + \frac{1}{4} + \tilde{C}(A) \right] \sqrt{\frac{U}{v_F}} \exp \left[ -\frac{2\pi v_F \tanh^{-1} A}{U} \frac{A}{A} \right], \quad (34)$$

where the Fermi velocity of the noninteracting chain is given by  $v_F = \frac{\sqrt{2}}{8} W(1 - \delta^2)/\sqrt{1 + \delta^2}$ ,  $A = (1 - \delta^2)/(1 + \delta^2)$  and  $\tilde{C}(A)$  is a function of  $A$ .<sup>38)</sup> We note that  $v_F$  depends on the total

bandwidth,  $W$ , while the temperature scale in the RG scheme is given in terms of the linearized bandwidth,  $E_0$ . Thus, we should bear in mind that there is arbitrariness in specification of the quantitative temperature scale corresponding to  $\Delta_{\rho 0}$ . In the case of  $W = 8E_0$  and  $U = 2.5t_{a1}$ , we estimate and show  $\delta$ -dependence of  $\Delta_{\rho 0}$ ,  $t_b^*$  and  $T_{\text{um}}$ , in the unit of  $t_{a1}$ , in Fig. 13.  $T_{\text{um}}$  is defined as the temperature scale at which the intrachain umklapp scattering strength,  $g_{3;l}$ , reaches unity. We see that two energy scales,  $\Delta_{\rho 0}$  and  $T_{\text{um}}$ , are close to each other. This fact indicates that growth of the umklapp scattering strength qualitatively corresponds to the preformation of the Mott gap.

We also comment on relevance of the present results to the confinement-deconfinement transition in terms of  $\Delta_{\rho 0}$  and  $t_{b0}$ .<sup>25,26,27)</sup> As is seen from Fig. 13,  $t_b^* > \Delta_{\rho 0}$  for smaller dimerization,  $\delta \leq 0.22$ . According to arguments given by Suzumura and Tsuchiizu<sup>25,26,27)</sup> for the coupled two half-filled chains, this fact might indicate that the incoherent metal regime for  $t_{b0} \lesssim t_b^*$  in the phase diagram of Fig. 11 belongs to the deconfinement regime. However, it is beyond the scope of this paper to reconcile the 2-loop RG flow of  $t_{b;l}$  determined by eqs. (15) and (16) with a possibility of the confinement in the present case of the infinite number of chains.

### 5.2 Misfit between the adjacent chains

We have not treated the misfit between the adjacent chains existing in the actual TMTTF and TMTSF crystals, which causes two kinds of interchain one-particle hopping integrals.<sup>39)</sup> In the FL regime,  $t_{b0} > t_b^*$ , it is straightforward to take account of the misfit by starting with the corresponding one-particle dispersion.<sup>5)</sup> On the other hand, serious treatment of the misfit effects in the incoherent metal regime is beyond the scope of the RG analysis, since we take a continuum limit along the  $a$ -axis in the RG analysis. It would be essential to take account of the misfit effects in both the two regimes to clarify the reason why the experimentally suggested SDW vector of  $(\text{TMTSF})_2\text{PF}_6$  is  $(1/2, 0.24 \pm 0.03, -0.06 \pm 0.20)$ ,<sup>40)</sup> while that of  $(\text{TMTTF})_2\text{Br}$  is  $(1/2, 1/4, 0)$ ,<sup>41)</sup> in the unit of the reciprocal lattice constants,  $a^*$ ,  $b^*$  and  $c^*$ .

### 5.3 Effects of the nearest-neighbor Coulomb repulsion

We comment on the effects of the intrachain nearest-neighbor Coulomb repulsion,  $V$ . In the present paper, we have not considered  $V$ , since the nature of the SDW transition approached *from the metallic side* is insensitive to  $V$  in the following reason. In the 1D regime, as far as the low-energy asymptotics of the system without  $t_{b0}$  is a Mott insulator, the presence of  $V$  only modifies the unrenormalized values of the scattering strengths, (10). In the FL regime, the SDW phase transition determined through the RPA condition, (31), is insensitive to  $V$ , unless  $V$  is too large to destabilize the SDW phase transition. We note that the effects of  $V$  and the next-nearest-neighbor repulsion,  $V_2$ , become important, if we clarify the *real space structure* of the spin and charge ordering *inside* the SDW phase.<sup>42,43)</sup>

## §6. Summary

In this work, we have studied the SDW phase transitions in the dimerized quarter-filled chains weakly coupled via the interchain one-particle hopping,  $t_{b0}$ . It is shown that there exists a critical value of  $t_{b0}$ ,  $t_b^*$ , between the incoherent metal regime ( $t_{b0} < t_b^*$ ) and the Fermi liquid regime ( $t_{b0} > t_b^*$ )

in the metallic phases above the SDW transition temperature. For  $t_{b0} < t_b^*$ , we assumed that the scaling hypothesis in the 1D regime works well down to the transition temperature,  $T_N^{\text{RG}}$ , and discussed the ICEX-driven SDW phase transition from the incoherent metal phase, based solely on the 2-loop RG flows. In our formulation, growth of the umklapp scattering toward low temperatures, which is regarded as the preformation of the 1D Mott gap, plays an essential role on occurrence of the SDW phase transition from the incoherent metal phase.

On the other hand, for  $t_{b0} > t_b^*$ , the system undergoes the crossover to the FL regime around the temperature,  $T_{\text{cross}}$ . In this case, the increasing  $t_{b0}$  weakens the degree of nesting of the Fermi surface and consequently decreases the nesting-driven SDW phase transition temperature.

### Acknowledgements

We acknowledge fruitful discussions with Y. Suzumura, M. Tsuchiizu, H. Kino, H. Kontani and T. Nakamura. This work was supported by a Grant-in-Aid for Encouragement of Young Scientists from the Ministry of Education, Science, Sports and Culture, Japan.

### Appendix: Derivation of the Renormalization-Group Equations

The renormalization-group procedure is best formulated in the path-integral representation of the partition function,<sup>20)</sup>

$$Z = \int \mathcal{D}e^S, \quad (\text{A}\cdot1)$$

where  $S$  is the action of the system and  $\mathcal{D}$  symbolizes the measure of the path-integral over the fermionic Grassmann variables. The action at the energy scale specified by  $l$  contains the four parts corresponding to the equation, (5),

$$S = S_a^{(1)} + S_a^{(2)} + S_b^{(1)} + S_b^{(2)}, \quad (\text{A}\cdot2)$$

which are give by

$$S_{a;l}^{(1)} = \sum_{k_a \in \mathcal{C}_l} \sum_{-\pi \leq k_b \leq \pi} \sum_{\varepsilon} \sum_{\sigma} \left[ \mathcal{G}_R^{-1}(K_a) R_{\sigma}^*(K) R_{\sigma}(K) + \mathcal{G}_L^{-1}(K_a) L_{\sigma}^*(K) L_{\sigma}(K) \right], \quad (\text{A}\cdot3)$$

$$S_{b;l}^{(1)} = 2 \sum_m \sum_{k_a \in \mathcal{C}_l} \sum_{-\pi \leq k_{bi} \leq \pi} \sum_{\varepsilon} \sum_{\sigma} (t_{b;l} \cos k_b - t'_{b;l} \cos 2k_b) [L_{\sigma}^*(K) L_{\sigma}(K) + R_{\sigma}^*(K) R_{\sigma}(K)], \quad (\text{A}\cdot4)$$

$$S_{a;l}^{(2)} = -\frac{\pi v_F T}{N_a N_b} \sum_{k_{ai} \in \mathcal{C}_l} \sum_{-\pi \leq k_{bi} \leq \pi} \sum_{\varepsilon_i, \sigma_i} g_l^{\sigma_1 \sigma_2 \sigma_3 \sigma_4} R_{\sigma_1}^*(K_1) L_{\sigma_2}^*(K_2) L_{\sigma_3}(K_3) R_{\sigma_4}(K_4) \\ - \frac{\pi v_F T}{2 N_a N_b} \sum_{k_{ai} \in \mathcal{C}_l} \sum_{-\pi \leq k_{bi} \leq \pi} \sum_{\varepsilon_i, \sigma, \sigma'} g_{3;l} [R_{\sigma}^*(K_1) R_{\sigma'}^*(K_2) L_{\sigma'}(K_3) L_{\sigma}(K_4) + \text{c.c.}], \quad (\text{A}\cdot5)$$

$$S_{b;l}^{(2)} = -\frac{\pi v_F T}{N_a N_b} \sum_Q J_{q_b;l} \mathbf{S}_l(q_a, q_b, \omega) \cdot \mathbf{S}_l^*(q_a, q_b, \omega) \\ - \frac{\pi v_F T}{N_a N_b} \sum_Q K_{q_b;l} [\mathbf{S}_l(2k_F + q_a, q_b, \omega) \cdot \mathbf{S}_l(2k_F - q_a, -q_b, -\omega) + \text{c.c.}], \quad (\text{A}\cdot6)$$

where  $R_{m,\sigma}$  and  $L_{m,\sigma}$  are Grassman variables representing the right- and left-moving electrons, respectively,  $K_a = (k_a, \varepsilon)$  and  $K = (k_a, k_b, \varepsilon)$  with  $\varepsilon$  being a fermion thermal frequency. The

intrachain one-particle propagator is given by

$$\mathcal{G}_\nu(K_a) = [\mathrm{i}\varepsilon - \xi_\nu(k_a)]^{-1}. \quad (\text{A.7})$$

We split up the set of  $k_a$ -points,  $\mathcal{C}_l$ , into two subsets as  $\mathcal{C}_l = \mathcal{C}_{l+\mathrm{dl}}^< \oplus d\mathcal{C}_{l+\mathrm{dl}}^>$ , where  $\mathcal{C}_{l+\mathrm{dl}}^< \equiv \{k_a \parallel \xi_\nu(k_a) \leq \omega_{l+\mathrm{dl}}/2\}$  and  $d\mathcal{C}_{l+\mathrm{dl}}^> \equiv \{k_a \mid \omega_{l+\mathrm{dl}}/2 \leq |\xi_\nu(k_a)| \leq \omega_l/2\}$ , represent the low- and high-energy shells, respectively. Accordingly, the action is decomposed as  $S_l = S_{l+\mathrm{dl}}^< + S_{l+\mathrm{dl}}^>$ . Integration over the modes in the high-energy shell gives

$$Z = \int_{\mathcal{C}_{l+\mathrm{dl}}^<} \mathcal{D} \exp \left[ S_{l+\mathrm{dl}}^< + \sum_{p,q,r=1}^{\infty} \Gamma_{pqr} \right], \quad (\text{A.8})$$

where  $\int_{\mathcal{C}_{l+\mathrm{dl}}^<} \mathcal{D}$  means that the Fermion momenta are restricted to the low-energy shell. All the renormalization effects come from the perturbative expansion

$$\Gamma_{pqr} = \frac{1}{p!q!r!} \langle\langle [S_{a;l+\mathrm{dl}}^{(2)>}]^p [S_{b;l+\mathrm{dl}}^{(1)>}]^q [S_{b;l+\mathrm{dl}}^{(2)>}]^r \rangle\rangle_c. \quad (\text{A.9})$$

The average over the modes in the high-energy shell is defined as  $\langle\langle (\cdots) \rangle\rangle = Z_{>}^{-1} \int_{d\mathcal{C}_{l+\mathrm{dl}}^>} \mathcal{D} \exp[S_{a;l+\mathrm{dl}}^{(1)>}] (\cdots)$ ,

with  $Z_{>} = \int_{d\mathcal{C}_{l+\mathrm{dl}}^>} \mathcal{D} \exp[S_{a;l+\mathrm{dl}}^{(1)>}]$  and the subscript 'c' represents the connected diagrams. We perform a perturbative expansion by picking up the Feynmann diagrams whose contribution is in proportion to  $\mathrm{dl}$  and then replacing  $S_{l+\mathrm{dl}}^< + \sum_{p,q,r=1}^{\infty} \Gamma_{p,q,r}$  with the renormalized action.

Then the renormalized action is written in the form,

$$\begin{aligned} \tilde{S}_{l+\mathrm{dl}}^< &= \sum_{k_a \in \mathcal{C}_{l+\mathrm{dl}}} \sum_{-\pi \leq k_b \leq \pi} \sum_{\varepsilon} \sum_{\sigma} [1 + \theta_l \mathrm{dl}] \\ &\quad \left[ \mathcal{G}_R^{-1}(K_a) R_\sigma^*(K) R_\sigma(K) + \mathcal{G}_L^{-1}(K_a) L_\sigma^*(K) L_\sigma(K) \right] \\ &+ 2 \sum_m \sum_{k_a \in \mathcal{C}_{l+\mathrm{dl}}} \sum_{-\pi \leq k_{bi} \leq \pi} \sum_{\varepsilon} \sum_{\sigma} (t_{b;l} \cos k_b - t'_{b;l} \cos 2k_b) [L_\sigma^*(K) L_\sigma(K) + R_\sigma^*(K) R_\sigma(K)] \\ &- \frac{\pi v_F}{N_a N_b} \sum_{k_{ai} \in \mathcal{C}_{l+\mathrm{dl}}} \sum_{-\pi \leq k_{bi} \leq \pi} \sum_{\varepsilon_i, \sigma_i} [g_l^{\sigma_1 \sigma_2 \sigma_3 \sigma_4} + w_l^{\sigma_1 \sigma_2 \sigma_3 \sigma_4} \mathrm{dl}] R_{\sigma_1}^*(K_1) L_{\sigma_2}^*(K_2) L_{\sigma_3}(K_3) R_{\sigma_4}(K_4) \\ &- \frac{\pi v_F}{2N_a N_b} \sum_{k_{ai} \in \mathcal{C}_{l+\mathrm{dl}}} \sum_{-\pi \leq k_{bi} \leq \pi} \sum_{\varepsilon_i, \sigma, \sigma'} [g_{3;l} + w_{3;l} \mathrm{dl}] [R_\sigma^*(K_1) R_{\sigma'}^*(K_2) L_{\sigma'}(K_3) L_\sigma(K_4) + \text{c.c.}] \\ &- \frac{\pi v_F}{N_a N_b} \sum_Q [f_{q_b;l}^J \mathrm{dl} + w_{q_b;l}^J J_{q_b;l} \mathrm{dl}] \mathbf{S}_{l+\mathrm{dl}}(q_a, q_b, \omega) \cdot \mathbf{S}_{l+\mathrm{dl}}^*(q_a, q_b, \omega) \\ &- \frac{\pi v_F}{N_a N_b} \sum_Q [f_{q_b;l}^K \mathrm{dl} + w_{q_b;l}^K K_{q_b;l} \mathrm{dl}] [\mathbf{S}_{l+\mathrm{dl}}(2k_F + q_a, q_b, \omega) \cdot \mathbf{S}_{l+\mathrm{dl}}(2k_F - q_a, -q_b, -\omega) + \text{c.c.}], \end{aligned} \quad (\text{A.10})$$

with

$$w_l^{\sigma_1 \sigma_2 \sigma_3 \sigma_4} = \delta_{\sigma_1 \sigma_4} \delta_{\sigma_2 \sigma_3} w_{2;l} - \delta_{\sigma_1 \sigma_3} \delta_{\sigma_2 \sigma_4} w_{1;l}. \quad (\text{A.11})$$

Next, to restore the original cutoff, we rescale the momenta and frequencies as  $\tilde{K}_a = e^{\mathrm{dl}} K_a$ . Here we note that the wave number in the  $b$ -axis direction is *not* rescaled. We perform the field-renormalization as

$$\tilde{R}_\sigma(\tilde{K}) = [1 + \frac{1}{2}(\theta_l - 3)\mathrm{dl}] R_\sigma(K), \quad (\text{A.12})$$

with  $\tilde{K} = (\tilde{k}_x, k_y, \tilde{\varepsilon})$ , and rewrite  $\tilde{S}_{l+\text{dl}}^<$  as

$$\begin{aligned}
\tilde{S}_{l+\text{dl}}^< &= \sum_{\tilde{k}_a \in \mathcal{C}_l} \sum_{k_b, \tilde{\varepsilon}, \sigma} \left[ \mathcal{G}_R^{-1}(\tilde{K}_a) R_\sigma^*(\tilde{K}) R_\sigma(\tilde{K}) + \mathcal{G}_L^{-1}(\tilde{K}_a) L_\sigma^*(\tilde{K}) L_\sigma(\tilde{K}) \right] \\
&+ 2 \sum_m \sum_{\tilde{k}_a \in \mathcal{C}_{l+\text{dl}}} \sum_{k_{bi}, \tilde{\varepsilon}, \sigma} (1 - \theta_l \text{dl}) (t_{b;l} \cos k_b - t'_{b;l} \cos 2k_b) \left[ L_\sigma^*(\tilde{K}) L_\sigma(\tilde{K}) + R_\sigma^*(\tilde{K}) R_\sigma(\tilde{K}) \right] \\
&- \frac{\pi v_F}{N_a N_b} \sum_{\tilde{k}_{ai} \in \mathcal{C}_l} \sum_{k_{bi}, \tilde{\varepsilon}_i, \sigma_i} [g_l^{\sigma_1 \sigma_2 \sigma_3 \sigma_4} + (w_l^{\sigma_1 \sigma_2 \sigma_3 \sigma_4} - 2\theta_l g_l^{\sigma_1 \sigma_2 \sigma_3 \sigma_4}) \text{dl}] R_{\sigma_1}^*(\tilde{K}_1) L_{\sigma_2}^*(\tilde{K}_2) L_{\sigma_3}(\tilde{K}_3) R_{\sigma_4}(\tilde{K}_4) \\
&- \frac{\pi v_F}{2N_a N_b} \sum_{\tilde{k}_{ai} \in \mathcal{C}_l} \sum_{k_{bi}, \tilde{\varepsilon}_i, \sigma, \sigma'} [g_{3;l} + (w_{3;l} - 2\theta_l g_{3;l}) \text{dl}] \left[ R_\sigma^*(\tilde{K}_1) R_{\sigma'}^*(\tilde{K}_2) L_{\sigma'}(\tilde{K}_3) L_\sigma(\tilde{K}_4) + \text{c.c.} \right] \\
&- \frac{\pi v_F}{N_a N_b} \sum_{\tilde{Q}} \left[ J_{q_b;l} + (w_{q_b;l}^J - 2\theta_l J_{q_b;l}) \text{dl} \right] \mathbf{S}_l(\tilde{q}_a, q_b, \omega) \cdot \mathbf{S}_l^*(\tilde{q}_a, q_b, \omega) \\
&- \frac{\pi v_F}{N_a N_b} \sum_Q \left[ K_{q_b;l} + (w_{q_b;l}^K - 2\theta_l K_{q_b;l}) \text{dl} \right] [\mathbf{S}_l(2k_F + \tilde{q}_a, q_b, \omega) \cdot \mathbf{S}_l(2k_F - \tilde{q}_a, -q_b, -\omega) + \text{c.c.}]
\end{aligned} \tag{A.13}$$

By identifying the renormalized quantities with the quantities at the energy scale specified by  $l + \text{dl}$ , we obtain

$$g_{l+\text{dl}}^{\sigma_1 \sigma_2 \sigma_3 \sigma_4} = g_l^{\sigma_1 \sigma_2 \sigma_3 \sigma_4} + (w_l^{\sigma_1 \sigma_2 \sigma_3 \sigma_4} - 2\theta_l g_l^{\sigma_1 \sigma_2 \sigma_3 \sigma_4}) \text{dl}, \tag{A.14}$$

$$g_{3;l+\text{dl}} = g_{3;l} + (w_{3;l} - 2\theta_l g_{3;l}) \text{dl}, \tag{A.15}$$

$$t_{b;l+\text{dl}} = t_{b;l} (1 - \theta_l \text{dl}), \tag{A.16}$$

$$t'_{b;l+\text{dl}} = t'_{b;l} (1 - \theta_l \text{dl}), \tag{A.17}$$

$$J_{q_b;l+\text{dl}} = J_{q_b;l} + (w_{q_b;l}^J - 2\theta_l J_{q_b;l}) \text{dl}, \tag{A.18}$$

$$K_{q_b;l+\text{dl}} = K_{q_b;l} + (w_{q_b;l}^K - 2\theta_l K_{q_b;l}) \text{dl}. \tag{A.19}$$

In Figs. 4 and 6, we show the 2-loop diagrams which contribute to  $\theta_l$  [Fig. 4],  $w_{q_b;l}^J$  [Fig. 6(a)] and  $w_{q_b;l}^K$  [Fig. 6(b)], respectively. In the intrachain self-energy corrections ( $\theta_l$ ) and the intrachain vertex corrections ( $w_l^{\sigma_1 \sigma_2 \sigma_3 \sigma_4}$  and  $w_{3;l}$ ), we neglect the contributions from the interchain interaction. It should be also noted that there are no 2-loop contributions to  $w_{q_b;l}^J$  and  $w_{q_b;l}^K$  because of the constraint on the chain indices for the 3rd order diagrams. After lengthy but straightforward manipulation, we obtain the following expressions,

$$\theta_l = \frac{1}{4} \left[ g_{1;l}^2 + g_{2;l}^2 - g_{1;l} g_{2;l} + g_{3;l}^2/2 \right], \tag{A.20}$$

$$w_{1;l} - 2\theta_l g_{1;l} = -g_{1;l}^2 - g_{1;l}^3/2, \tag{A.21}$$

$$w_{2;l} - 2\theta_l g_{2;l} = -\frac{1}{2} g_{1;l}^2 + g_{3;l}^2/2 - g_{1;l}^3/4 + g_{3;l}^2 (g_{1;l} - 2g_{2;l})/4, \tag{A.22}$$

$$w_{3;l} - 2\theta_l g_{3;l} = g_{3;l} (g_{1;l} - 2g_{2;l}) [1 + (g_{1;l} - 2g_{2;l})/4] - g_{3;l}^3/4, \tag{A.23}$$

$$\begin{aligned}
w_{q_b;l}^J - 2\theta_l J_{q_b;l} &= \frac{1}{2} \left[ g_{2;l}^2 + 4g_{3;l}^2 \right] f_l(q_b) \\
&+ \frac{1}{2} [(g_{2;l} - 4\theta_l) J_{q_b;l} + 4g_{3;l} K_{q_b;l}] - \frac{1}{4} \left[ J_{q_b;l}^2 + 4K_{q_b;l}^2 \right],
\end{aligned} \tag{A.24}$$

$$w_{q_b;l}^K - 2\theta_l K_{q_b;l} = 2g_{2;l} g_{3;l} f_l(q_b) + 2 [(g_{2;l} - \theta_l) K_{q_b;l} + g_{3;l} J_{q_b;l}] - J_{q_b;l} K_{q_b;l}, \tag{A.25}$$

which give the RG equations (15), (16), (19)  $\sim$  (21), (25) and (26). The terms including  $\theta_l$  in (A.24) and (A.25) come from the field-renormalization due to the intrachain self-energy processes and give negligibly small corrections to the solutions.

---

- [1] For example, see T. Ishiguro, G. Saito, K. Yamaji, *Organic Superconductors* (Springer Series in Solid-State Sciences, 88), (1998).
- [2] C. S. Jacobsen, D. B. Tanner, K. Bechgaard, *Phys. Rev. Lett.* **46** (1981) 1142.
- [3] V. Vescoli, L. Degiorgi, W. Henderson, G. Grüner, K.P. Starkey and L.K. Montgomery, *Science* **281**(1998)1181.
- [4] V. J. Emery, R. Bruinsma and S. Barisic, *Phys. Rev. Lett.* **48** (1982) 1039.
- [5] K. Yamaji, *J. Phys. Soc. Jpn.* **51** (1982) 2787.
- [6] Y. Hasegawa and H. Fukuyama, *J. Phys. Soc. Jpn.* **55** (1986) 3978.
- [7] H. Shimahara, *J. Phys. Soc. Jpn.* **58** (1989) 1735.
- [8] J. Moser, M. Gabay, P. Auban-Senzier, D. Jerome, K. Bechgaard and J.M. Fabre, *Eur. Phys. J.* **B1** (1998) 39.
- [9] A. Schwartz, M. Dressel, G. Grüner, V. Vescoli, L. Degiorgi and T. Giamarchi, *Phys. Rev. B* **58** (1998) 1261.
- [10] P. Fertey, M. Poirier and P. Batail, preprint, cond-mat/9901331.
- [11] L. P. Gor'kov and A. G. Lebed', *J. Phys. Lett. (France)* **45** (1984) L433.
- [12] K. Yamaji, *J. Phys. Soc. Jpn.* **54** (1985) 1034.
- [13] T. Osada, N. Miura and G. Saito, *Physica* **143B** (1986) 403.
- [14] B. J. Klemme, S. E. Brown, P. Wzietek, D. Jerome and J. M. Fabre, *J.Phys. I France* **6** (1996) 1745.
- [15] M. Hisano, T. Nakamura, T. Takahashi and G. Saito, to appear in *Synth. Met.*
- [16] J. Sólyom, *Adv. Phys.* **28** (1979) 201.
- [17] K. Penc and F. Mila, *Phys. Rev. B* **50** (1994)11429.
- [18] S. A. Brazovskii and V. M. Yakovenko, *Sov. Phys. JETP* **62** (1985) 1340.
- [19] Y. Suzumura, *J. Phys. Soc. Jpn.* **24** (1982) 2386.
- [20] C. Bourbonnais and L. G. Caron, *Int. J. Mod. Phys. B* **5** (1991) 1033.
- [21] C. Bourbonnais, *J.Phys. I France* **3** (1993) 143.
- [22] C. Bourbonnais, in *Strongly Interacting Fermions and High  $T_c$  Superconductivity*, ed. B. Doucot and J. Zinn-Justin(Elsevier, Amsterdam, 1995), p. 307.
- [23] C. Bourbonnais, *Synth. Met.* **84** (1997) 19.
- [24] T. Giamarchi, *Physica B* **230-232** (1997) 975.
- [25] Y. Suzumura, M. Tsuchiiizu and G. Grüner, *Phys. Rev. B* **57** (1998) R15040.
- [26] M. Tsuchiiizu, Y. Suzumura and T. Giamarchi, *Prog. Theor. Phys.* **101** (1999) 763.
- [27] M. Tsuchiiizu, Y. Suzumura, preprint, cond-mat/9903135.
- [28] J. Kishine and K. Yonemitsu, cond-mat/9807153, to appear in *Synth. Met.*
- [29] K. Yamaji, *J. Phys. Soc. Jpn.* **52** (1983) 1361.
- [30] Recall that the 1D non interacting retarded one-particle propagator is given by  $\mathcal{G}_R(x, t = 0) \propto \frac{1}{\xi \sinh[x/\xi]}$ , which behaves as  $x^{-1}$  for  $x \ll \xi$ , while  $e^{-x/\xi}$  for  $x \gg \xi$ .
- [31] J. Kishine and K. Yonemitsu, *J. Phys. Soc. Jpn.* **67** (1998) 2590.
- [32] M. Kimura, *Prog. Theor. Phys.* **53** (1975) 955.
- [33] D. Boies, C. Bourbonnais and A.-M.S Tremblay, *Phys. Rev. Lett.* **74** (1995) 968.
- [34] D. J. Scalapino, Y. Imry and P. Pincus, *Phys. Rev. B* **11** (1975) 2042.
- [35] H. Kino and H. Kontani, submitted to *J. Phys. Soc. Jpn.*
- [36] F. Mila, *Phys. Rev. B* **52** (1995) 4788.

- [37] M. Tsuchiizu, H. Yoshioka and Y. Suzumura, preprint.
- [38] See eq. (6.25) of ref. [17].
- [39] P. M. Grant, Journal de Physique, Colloque **C3** (1983) 847.
- [40] T. Takahashi, Y. Maniwa, H. Kawamura and G. Saito, J. Phys. Soc. Jpn. **55** (1986) 1364.
- [41] T. Nakamura, T. Nobutoki, Y. Kobayashi, T. Takahashi and G. Saito, Synth. Met. **70** (1995) 1293.
- [42] H. Seo and H. Fukuyama, J. Phys. Soc. Jpn. **66** (1997) 1249.
- [43] N. Kobayashi, M. Ogata and K. Yonemitsu, J. Phys. Soc. Jpn. **67** (1998) 1098.

Fig. 1. Array of dimerized quarter-filled Hubbard chains considered here.

Fig. 2. Broken lines represent the one-particle dispersion, (1), in the absence of  $t_{b0}$  and  $U$ .  $R$  and  $L$  are the linearized dispersions for the right- and left-moving electrons with the bandwidth cutoff  $E_0$ . At the energy scale,  $\omega_l = E_0 e^{-l}$ , we observe the system.

Fig. 3. Fundamental processes considered here. The solid and broken lines represent the propagators for the right- and left-moving electrons, respectively. The zigzag line in (a) represents the interchain one-particle hopping process. Single and double wavy lines in (b), (c) and (d) represent the intrachain “normal” and “umklapp” scattering, respectively. White and black squares in (e) and (f) represent the interchain interaction between the  $i$ -th and  $j$ -th chains in the antiferromagnetic channel, due to the normal (e) and umklapp (f) processes.

Fig. 4. Renormalization of the interchain one-particle propagation through the self-energy processes.

Fig. 5. RG flows of  $t_{b;l}$  for dimerization ratios,  $\delta = 0, 0.2, 0.4, 0.8$ .

Fig. 6. Renormalization of the ICEX processes in the AF channel for the (a) normal and (b) umklapp processes.

Fig. 7. RG flows of  $g_{3;l}$ ,  $t_{bl}/E_0$ ,  $J_{qb;l}$  and  $K_{qb;l}$  with  $qb = \pi$  for  $\delta = 0.2$  and  $t_{b0}/E_0 = 0.02, 0.108, 0.3$ , where the vertical lines show the locations of  $l_{\text{cross}}$  and  $l_N$ .

Fig. 8. Dependence of  $t_b^*$  on the dimerization ratio  $\delta$  for  $U/\pi v_F = 1.0, 1.45, 1.6$ .

Fig. 9. A series of diagrams representing the particle-hole fluctuations which contribute to the transverse susceptibility within the RPA. The double solid and broken lines represent the two-dimensional one-particle propagators for the right- and left-moving sectors,  $\mathcal{G}_R^{2D}$  and  $\mathcal{G}_L^{2D}$ , respectively. The single and double wavy lines represent the intrachain  $g$ -ology interaction for the normal and umklapp processes, respectively.

Fig. 10. Dependence of  $T_N^{\text{RPA}}$  on  $t_{b0}$  for  $U = 1.45\pi v_F$  and  $\delta = 0.05, 0.2, 0.4$ .

Fig. 11. SDW phase diagram for  $U = 1.45\pi v_F$  and  $\delta = 0.2$ . **SDW (ICEX)** stands for the spin density wave phase driven by the interchain exchange process in the AF channel. **SDW (ND)** stands for the spin density wave phase driven by the Fermi surface nesting.

Fig. 12. SDW phase diagrams for dimerization ratios (a) smaller ( $\delta = 0.05$ ) or (b) larger ( $\delta = 0.6$ ) than that of Fig. 11.

Fig. 13.  $\delta$ -dependence of  $\Delta_{\rho 0}/t_{a1}$ ,  $t_b^*/t_{a1}$  and  $T_{\text{um}}/t_{a1}$  in the case of  $W = 8E_0$  and  $U = 2.5t_{a1}$ .

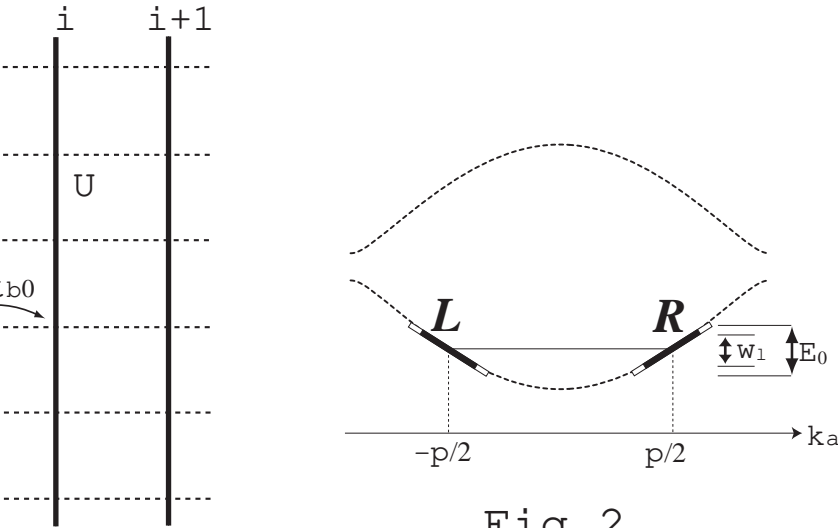


Fig. 2

Fig. 1

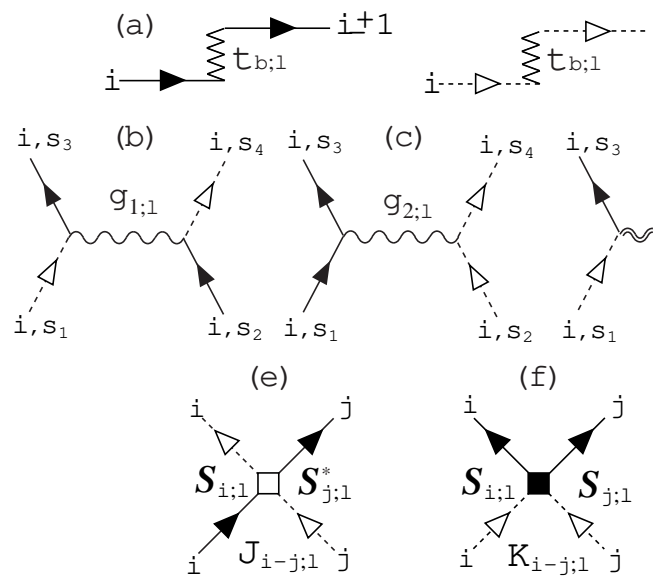


Fig. 3

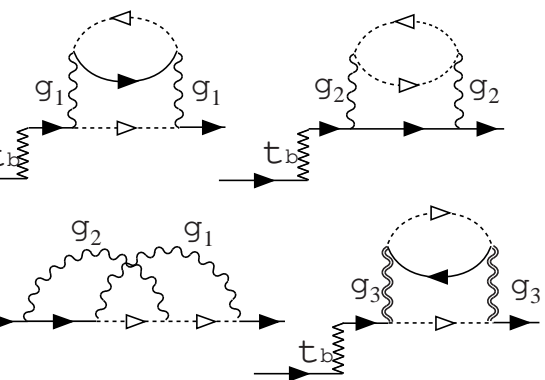


Fig. 4

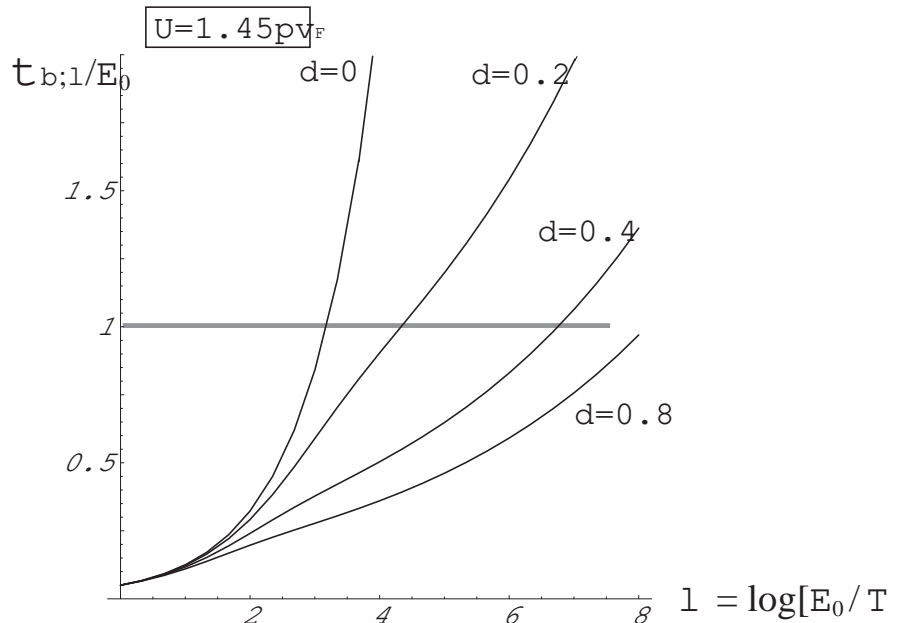


Fig. 5

J.Kishine and K.Yonemitsu

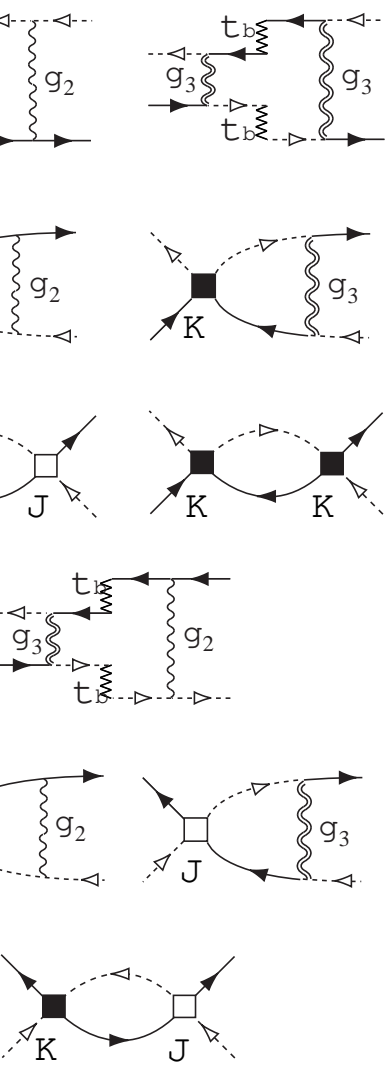


Fig. 6

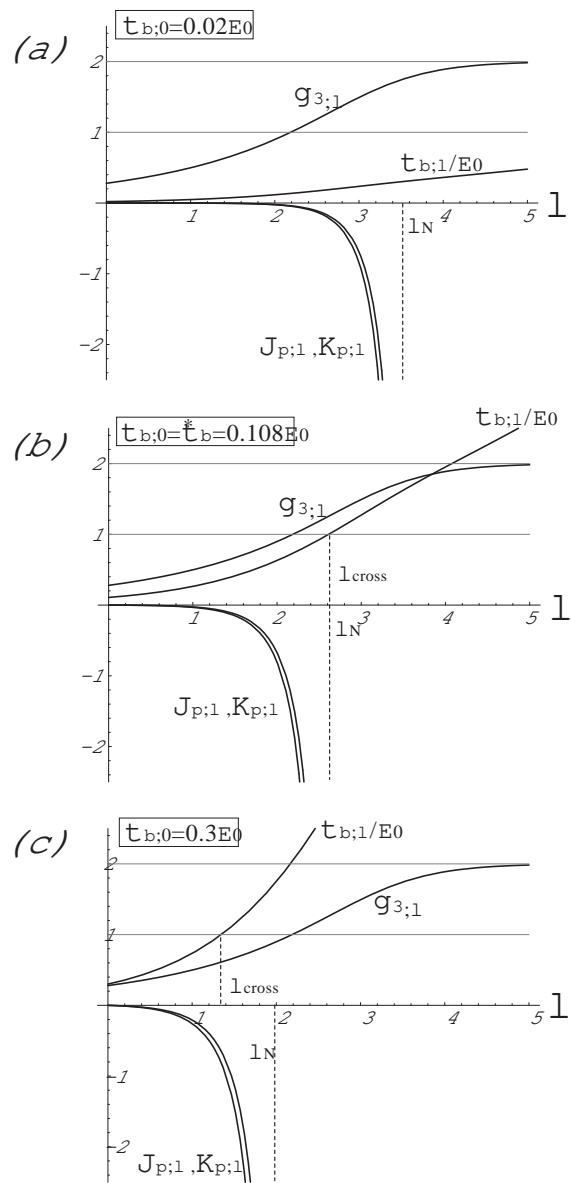


Fig. 7

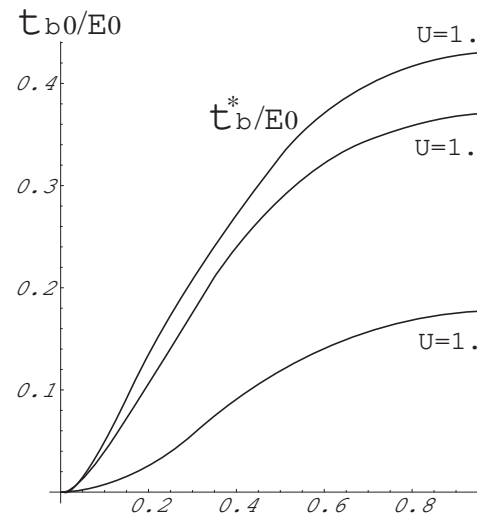


Fig. 8

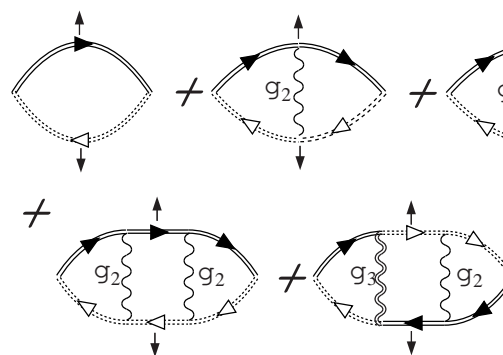


Fig. 9

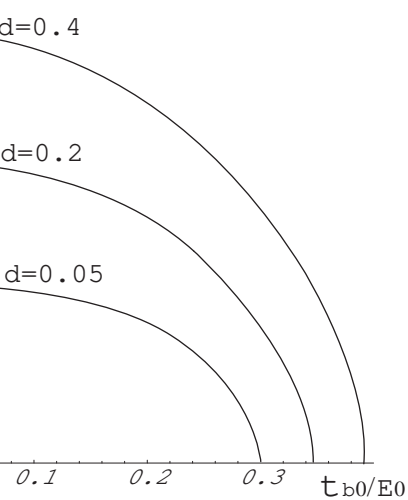


Fig.10

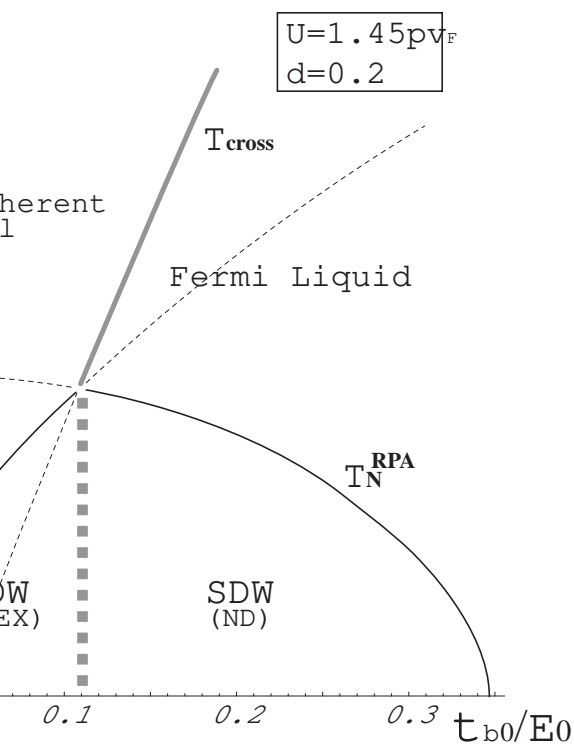


Fig.11

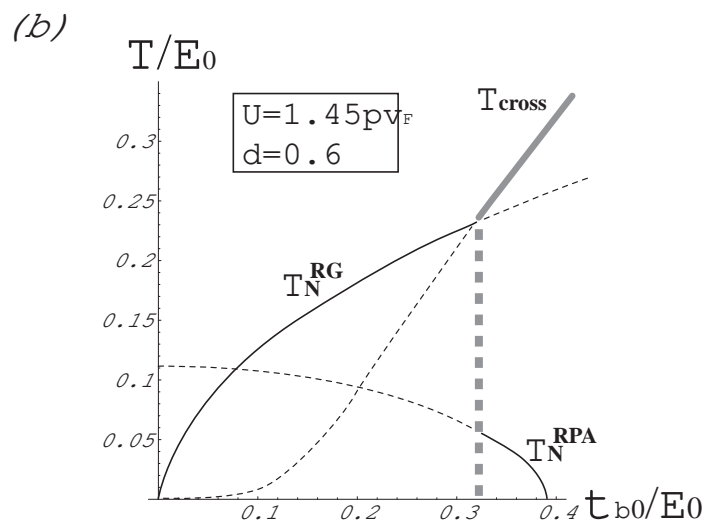
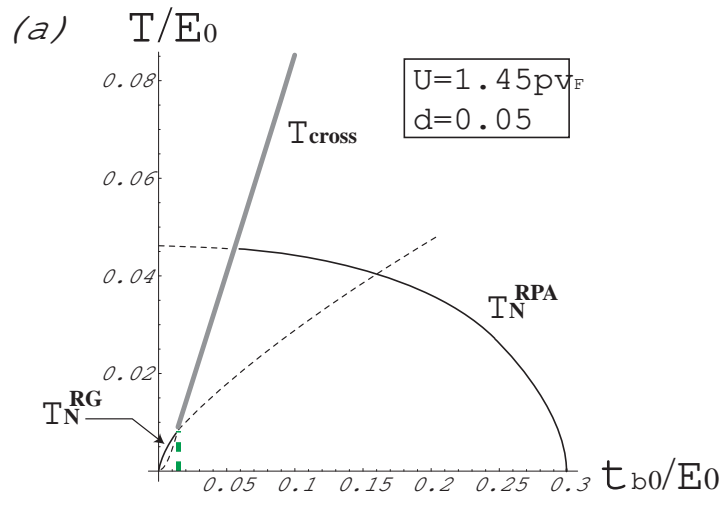


Fig.12

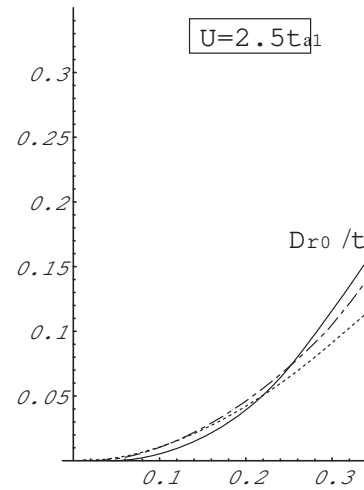


Fig.13